Project Report
TIP-141

Etched Black Electroless Nickel Coatings for Stray Light Control: FY20 Engineering Research Technical Investment Program

C.D. Roll
K.E. Krueger

3 February 2021

Lincoln Laboratory
MASSACHUSETTS INSTITUTE OF TECHNOLOGY
LEXINGTON, MASSACHUSETTS

DISTRIBUTION STATEMENT A. Approved for public release. Distribution is unlimited.

This report is the result of studies performed at Lincoln Laboratory, a federally funded research and development center operated by Massachusetts Institute of Technology. This material is based upon work supported by the United States Air Force under Air Force Contract No. FA8702-15-D-0001. Any opinions, findings, conclusions or recommendations expressed in this material are those of the author(s) and do not necessarily reflect the views of the United States Air Force.

© 2021 MASSACHUSETTS INSTITUTE OF TECHNOLOGY

Delivered to the U.S. Government with Unlimited Rights, as defined in DFARS Part 252.227-7013 or 7014 (Feb 2014). Notwithstanding any copyright notice, U.S. Government rights in this work are defined by DFARS 252.227-7013 or DFARS 252.227-7014 as detailed above. Use of this work other than as specifically authorized by the U.S. Government may violate any copyrights that exist in this work.

Massachusetts Institute of Technology
Lincoln Laboratory

Etched Black Electroless Nickel Coatings for Stray Light Control: FY20 Engineering Research Technical Investment Program

C.D. Roll
Group 74
K.E. Krueger
Group 72

Project Report TIP-141

3 February 2021

DISTRIBUTION STATEMENT A. Approved for public release. Distribution is unlimited.

This material is based upon work supported by the United States Air Force under Air Force Contract No. FA8702-15-D-0001.

Lexington Massachusetts

This page intentionally left blank.

ABSTRACT

Many Lincoln Laboratory prototypes require black surface coatings to meet optical requirements. Current options necessitate tradeoffs that limit system performance or sacrifice attributes such as environmental robustness, cost, and lead time. Etched black electroless nickel (EBEN) coatings exhibit the potential to minimize these tradeoffs. The research goal was to develop a robust process for creating EBEN coatings, characterize the coatings properties, and establish a new coating option ready for use in LL prototypes. While this work demonstrated the feasibility of EBEN techniques to create deep black surfaces, the process could not be reproduced reliably and is not currently recommended for MIT LL flight programs.

This page intentionally left blank.

TABLE OF CONTENTS

This page intentionally left blank.

LIST OF ILLUSTRATIONS

LIST OF ILLUSTRATIONS
(Continued)

LIST OF TABLES

This page intentionally left blank.

1. PROBLEM STATEMENT

A large number of systems developed at Lincoln Laboratory require black surface coatings to meet optical performance requirements. Aside from providing high absorption over large angles of incidence, these coatings need to be diffuse, low outgassing, and environmentally robust. In addition, cost and lead-time are often considerations. Laboratory programs generally select from a limited number of black coatings that require a compromise on one or more of these desired attributes. Finally, it is difficult and time consuming to implement a new coating that does not have previous flight heritage. Ultimately, this limits potential system performance for many advanced prototypes.

1.1 POTENTIAL IMPACT TO FUTURE MISSIONS

In 2018, the Mustang program evaluated a category of etched black electroless nickel (EBEN) coatings for use on its opto-mechanical components. Initial samples, based on existing literature, were produced and optically tested. Figure 1 shows total integrated scatter of the EBEN surface compared to other black coatings recently used at MIT LL. In particular, the optical performance is similar to Deep Space Black, which was used on the SensorSat baffle to control stray light in order to meet the imager's challenging signal to noise ratio requirement. However, Deep Space Black is made by a single supplier, has long lead times, limited substrate compatibility, is very fragile, and is expensive. In contrast, the EBEN is robust, inexpensive, and compatible with more substrate materials, while maintaining similar optical performance. This clearly indicates the potential impact to MIT LL programs. Unfortunately, the Mustang program did not have time to fully develop this coating technology before needing to down select to a lower performing coating to meet schedule needs.

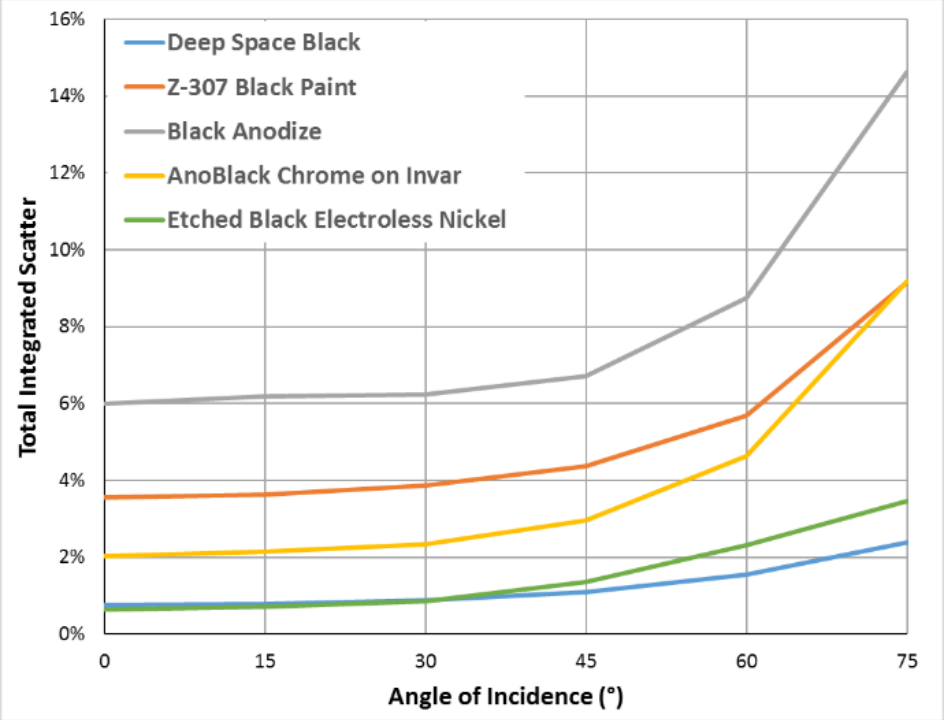

Figure 1. Total integrated scatter of black surfaces.

1.2 PROGRAMMATIC APPROACH

Existing literature and recent coating samples clearly indicate the feasibility of this etched black electroless nickel process. However, there is a gap between an experimental method and a robust process that has fully characterized results. This engineering research project leveraged and built upon the preliminary work started by the Mustang program attempting to bridge that gap. In addition, this initiative collaborated with local plating vendors to evaluate the feasibility of leveraging industry to replicate this process for future flight programs. This approach utilized the experimentation and prototyping expertise at the MIT LL as well as industry resources to search for a successful path to implementation.

2. LITERATURE REVIEW

The approach of generating ultra-black surfaces by etching nickel-phosphorus coatings (electroless nickel) was first published in 1980 and patented by Christian Johnson at the National Bureau of Standard (now NIST). He discovered that immersion of electroless nickel into a highly oxidizing nitric acid solution creates a surface microstructure of conical pores. This morphology is responsible for the high light-absorbing properties, which he demonstrated as greater than 99% of light over the wavelength range of 320 to 2140 nm. While he understood that the resulting surface properties depended on the specific nitric acid concentration, temperature, and immersion time, he did not rigorously test or determine the optimal set of parameters (Johnson, 1980).

More recently, others such as Brown, Brewer, & Milton (2002) at the National Physical Laboratory, and Saxena, Rani, & Sharma (2006) at the ISRO Satellite Center in India evaluated how the composition of the base electroless nickel plating and the etching process parameters impact the surface morphology and resulting absorptive properties. They optimized each factor and determined a similar set of parameters for maximizing the absorptive properties of the coatings, which are summarized in Table 1 below.

Table 1

Optimized Parameters for Ultra-Black Electroless Nickel Surfaces

Parameter	Optimized Value	Units
Plating Thickness	30 ± 2	µm
Phosphorous Concentration	5-7	% by Mass
Electroless Nickel pH	4.7	-
Acid Bath Composition	Nitric Acid [HNO_3]	-
Acid Bath Concentration	9	M
Acid Bath Temperature	40	°C
Immersion Time	40	s

These groups present very impressive results and demonstrate the high optical performance that can be achieved. However, the literature also indicates that the process can create non-uniform results. For example, Geikas mentions, "some difficulties have arisen on attempts to achieve uniform plating on large baffles" (Geikas, 1983, p. 18). In addition, inconsistency in the nickel plating may also be critical, as discussed by Brown, Brewer & Milton (2002):

> "…variability is a much more serious consideration when plating on an industrial scale, since additional factors such as the plate position in the bath, stirring efficiency and temperature

> distribution are of importance. We have noted that alloys produced on the industrial scale, even after fractional bath turnovers, can produce a range of reflectance values, even with approximately the same P content (as measured by EDX). We propose that such variability is due to differences in the structure of the as-plated Ni–P alloy. The presence of reaction products in the bath, the depletion of the active plating chemicals and changes in the effective bath loading are all thought to contribute to this phenomenon." (p. 2751)

Finally, another research group claims that the blackening process using HNO_3 occurs too quickly to adequately control, which results in non-uniform distribution of the conical pores that serve as light absorbing features. Ultimately, they propose a different blackening method using an anodic oxidation process with phosphoric acid (H_3PO_4). This alternative method will be discussed later in the report (Jin, Yang, Zeng, & Fu, 2015).

3. PROCESS DEVELOPMENT USING SMALL TEST COUPONS

3.1 MATERIALS AND METHODS

Initial testing was conducted using Invar 36 coupons, shown in Figure 2, with dimensions 1.5" x 1.5" x 0.1", each engraved with a serial number to facilitate tracking.

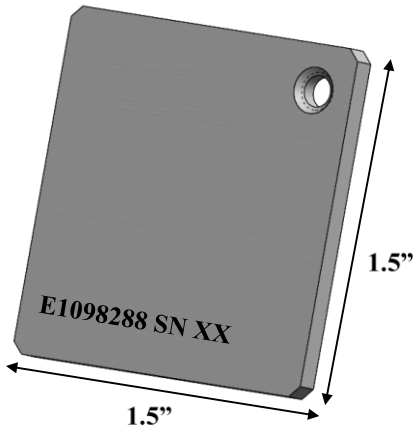

Figure 2. Small Invar 36 coupons.

The literature review along with previous experimentation conducted by the Mustang program provided a starting point to conduct the process development. The optimized process parameters detailed in Table 1 were used to specify the initial electroless nickel plating specifications as well as the parameters for conducting the etching and blackening step. The electroless nickel process is a capability that MIT LL does not have internally, but outside vendors are readily able to plate parts with EN in a controlled and repeatable fashion. AOTCO, located in Billerica, MA, is a standard supplier of metal finishes for MIT LL and was selected to plate the test samples with nickel. Separately, the blackening process occurred at MIT LL. An initial set of small, flat, Invar 36 coupons were plated and blackened while rigorously documenting process parameters in order to understand the sensitivities of each variable. Invar 36 was used to remain consistent with initial experimentation in 2018 and with the work documented by Saxena, Rani, & Sharma (2006).

3.2 SURFACE PREPARATION

Previous experimentation indicated that surface roughness improved the diffusivity of the blackened electroless nickel, which is beneficial for most stray light control applications. Therefore, the surfaces of the samples were prepared for plating by conducting a media blast in the MIT LL Group 72 Polymer Lab with two different media: 60 grit aluminum oxide (AlO_2) powder and 50 grit steel shot. The pre-plated surfaces were characterized using a Jeol JSM-IT100LA scanning electron microscope (SEM) to view the initial surface structure, which is shown in Figure 3. Next, a Mitutoyo SJ-410 surface profilomiter characterized the roughness of the front and back of each sample. Finally, the samples were cleaned and

weighed on a precision scale to provide a means for calculating an estimated plating thickness. The surface preparation details for each sample is provided in Table 2 below.

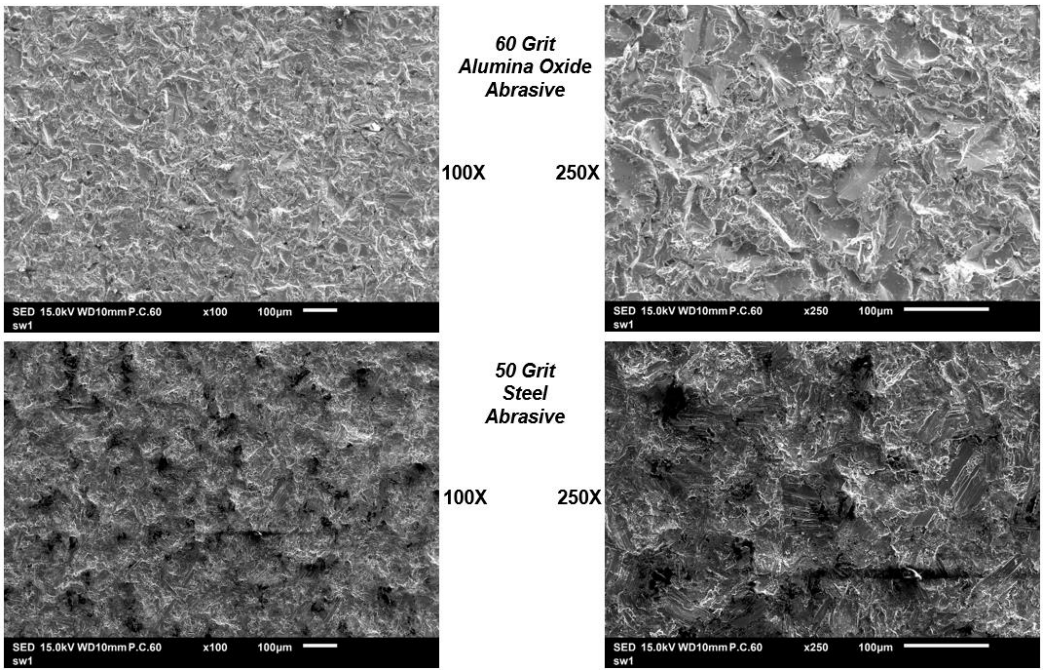

Figure 3. Sample surfaces prior to plating.

Table 2

Test Sample Surface Preparation and Electroless Nickel Plating Measurements

SN #	LOT #	Surface Prep		Age of Ni-P Bath	Measured Phosphorous Concentration	Nominal Electroless Ni Density*	Measured Thickness	Measured PH	Measured Temp	Post Media Blast Average Surface Roughness RA	Post Meadia Blast Mass	Post Electroless Nickel Mass	Estimate Plating Thickness
		[-]	[-]	[-]	[%]	[g/cm^2]	[in]	[-]	[°F]	[µin]	[g]	[g]	[µm]
3	1	Chemically Stripped by AOTCO	60 - Grit Aluminum Oxide	1/2 Cycle	5.6	8.3	32	5.2	187	106	29.809	30.748	34
4										115	29.866	30.820	35
6										104	29.853	30.793	35
8										119	29.883	30.846	35
9										109	29.905	30.850	35
20	2		50 - Grit Steel Media	1/2 Cycle	5.6		32	5.2	187	77	30.567	31.494	34
21										141	29.685	30.612	34
22										154	30.175	31.135	35
23										158	29.927	30.884	35
24										190	29.850	30.788	34
10	3	Chemically Stripped by AOTCO	60 - Grit Aluminum Oxide	1 1/2 Cycle	7.6	8.1	33	5.2	191	122	29.953	30.785	31
12										118	29.920	30.747	31
13										107	29.789	30.611	31
14										119	29.820	30.654	31
19										106	29.931	30.754	31
25	4		50 - Grit Steel Media	1 1/2 Cycle	7.6		33	5.2	195	173	30.110	30.941	31
26										161	29.720	30.542	31
27										153	29.280	30.085	30
28										154	29.658	30.484	31
29										160	29.788	30.613	31
5	5	Chemically Stripped by AOTCO	60 - Grit Aluminum Oxide	2 1/2 Cycle	6.8	8.2	33	5.2	193	111	30.060	31.203	42
18										110	29.632	30.808	44
32										114	29.926	31.063	42
33										112	29.570	30.725	43
34										108	29.791	-	-
35	6		50 - Grit Steel Media	2 1/2 Cycle	6.8		33	5.2	193	158	29.517	30.669	43
36										170	29.899	-	-
37										153	29.704	30.869	43
38										155	29.419	30.571	43
40										143	29.565	30.696	42

* *Estimated Electroless Ni density based on phosphorous content: https://industrial.macdermidenthone.com/products-and-applications/electroless-nickel/properties

3.3 ELECTROLESS NICKEL PLATING AND CHARACTERIZATION

As indicated in the literature review, variability in the electroless plating process can lead to variability in the final etched and blackened surface. The following plating parameters were recorded for each of the samples: age of the Ni-P bath, pH and temperature of the bath, phosphorous content and plating thickness. Samples were requested with three different Ni-P bath ages (1/2, 1½, and 2½ cycle) to evaluate the potential impact of this variable. It is costly to require a fresh plating bath for each lot of parts, or a schedule impact to wait for a plater to have a bath of specific age. Ideally, the process would be agnostic to this variable. After plating, the samples were sealed in nitrogen-purged plastic and delivered to MIT LL. The mass of the plated samples was measured again prior to conducting the etching step. The plating thickness for each sample was estimated from the nominal EN density (based on the measured phosphorous content of the plating bath), the total surface area of the samples, and the pre-plated mass of the samples.

To further characterize the EN plating, samples SN 34 and SN 36 were cross-sectioned, potted in resin, and polished to directly measure the plating thickness and the substrate-to-plating interface. Figure 4 shows the sectioned portion of SN 36 in the resin. SEM images of the sample cross-section are seen in Figure 5. The measured plating thickness of 40 µm closely matches the estimated thickness of the other samples from Lot 6 listed in the table above. It was however about 18% thicker than the 33 µm plating thickness that the vendor claimed.

Figure 4. Cross-section of sample SN 36 potted in resin and polished.

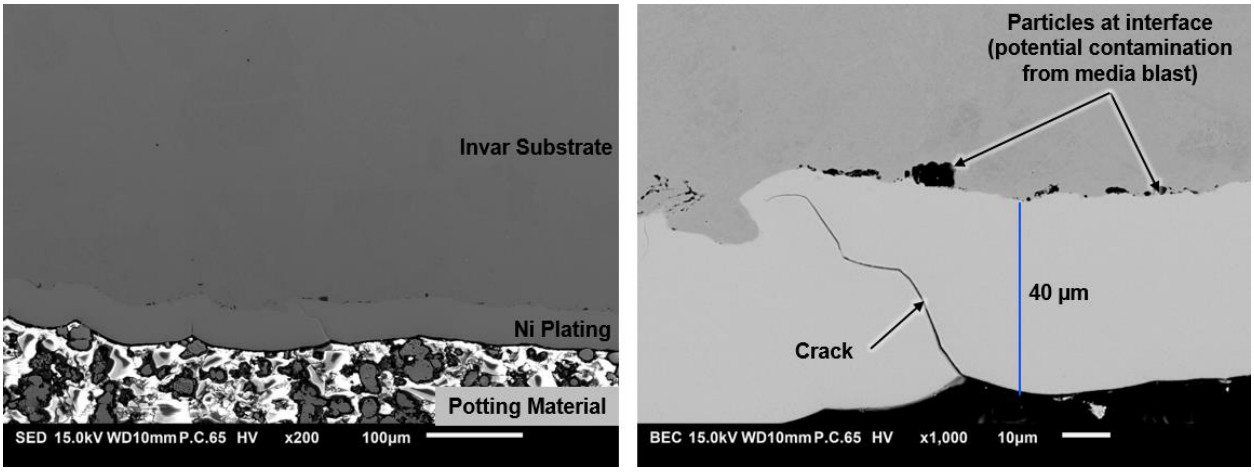

Figure 5. Cross-section SEM image of SN 36.

Next, the electroless nickel surfaces were also examined using the SEM. Figure 6 depicts significant surface differences between samples from Lot 3 and Lot 5. The image on the left shows surface cracks across the sample breaking the coating into almost a "tectonic plate-like" structure. The cross section image of SN 36 in Figure 5 appears to show that these cracks prorogate through a significant portion of the coating thickness. The image on the right shows a surface that is smooth and almost free off all surface cracks. Cosmetically, the samples from Lot 3 were noticeably brighter and shinier than the samples from Lot 5.

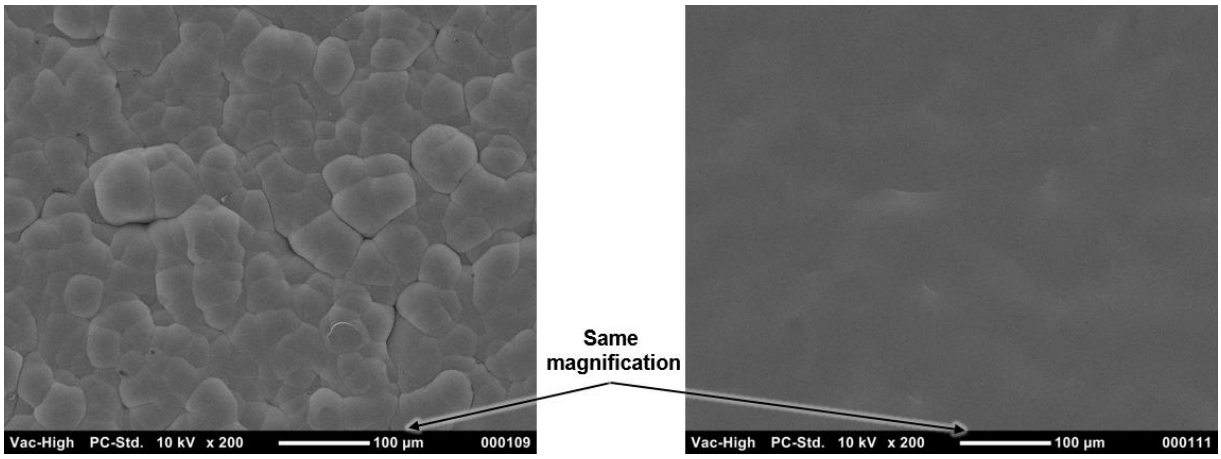

Figure 6. Electroless nickel surfaces of different sample lots. (Left) EN surface of SN 34, Lot 5 (Right) EN surface of SN 19, Lot 5.

The characterization of the electroless nickel plating showed that there was significant differences between the sample lots despite the goal minimizing variability to achieve reproducible black surfaces. Some of this could be attributed to the differing ages of the plating baths for these two lots, however, further testing would be necessary to make that conclusion.

The electroless nickel plating was further characterized using SEM energy dispersive x-ray spectroscopy (EDS) analysis to measure the nickel and phosphorous content of each sample. The literature suggested that that percent phosphorous content (by mass) was an important factor in the development of the surface morphology and a 5% and 7% was considered ideal (Brown, Brewer, & Milton, 2002). Again, Table 2 lists the phosphorous content for each lot of EN plated samples, as provided by the vendor. The cross-sectioned samples of SN 34 reveled 7.1% phosphorous (Figure 7) and SN 36 measured 6.9% (Figure 8). This closely correlates to the 6.8% plating bath phosphorous concentration measured by the vendor and is within the target range for optimum etching and blackening.

Since the SEM-EDS process is time consuming and expensive, it was not practical to measure each sample using this method. Instead, a Thermo Scientific XL3T handheld X-ray fluorescence instrument, was used to measure the EN plating composition prior to plating and after the etching process. For the XRF technique to accurately measure the composition, the coating thickness needs to meet the "infinite thickness" critera, where 99% of the input x-rays are absorbed by the sample. The XL3T datsheet indicates that this thickness is 20 µm for nickel on steel substrates. Since the coatings in question include phosphorous, which is a lighter element, the coating density decreases, and the "infinite thickness" increases according to the Beer-Labert Law. Therefore, the approximately 33 µm coating thickness prior to etching is likely not thick enough to provide accurate composition measurements with this instrument. For example, the SEM-EDS measurements and the vendor data indicated that sample lots 5 and 6 have 7% P concentration. However, the average P content for the samples in thoses lots as measured with the XL3T XRF was 4%. Despite this discrepancy, the XRF data was taken for all samples to provide a qualitiative comparision of the intial and final coating compositions.

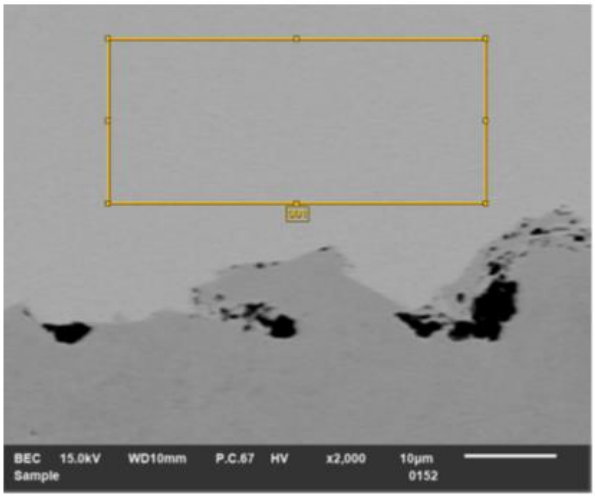

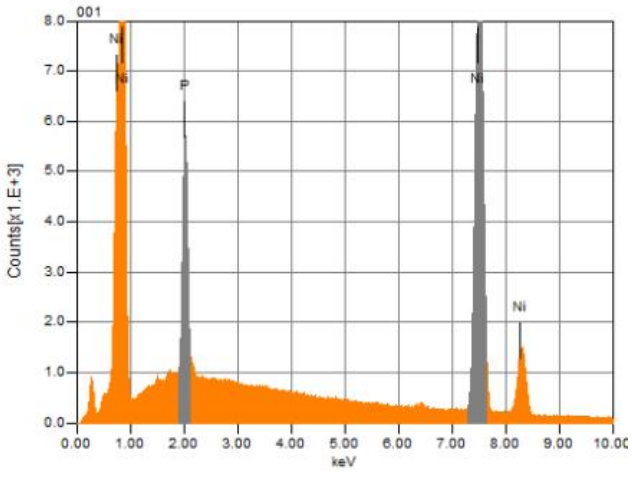

Formula	mass%	Atom%	Sigma	K ratio	Line
P	7.11	12.66	0.03	0.1811265	K
Ni*	92.89	87.34	0.18	3.4518139	K
Total	100.00	100.00			

Figure 7. EDS measurement of SN 34 electroless nickel plating.

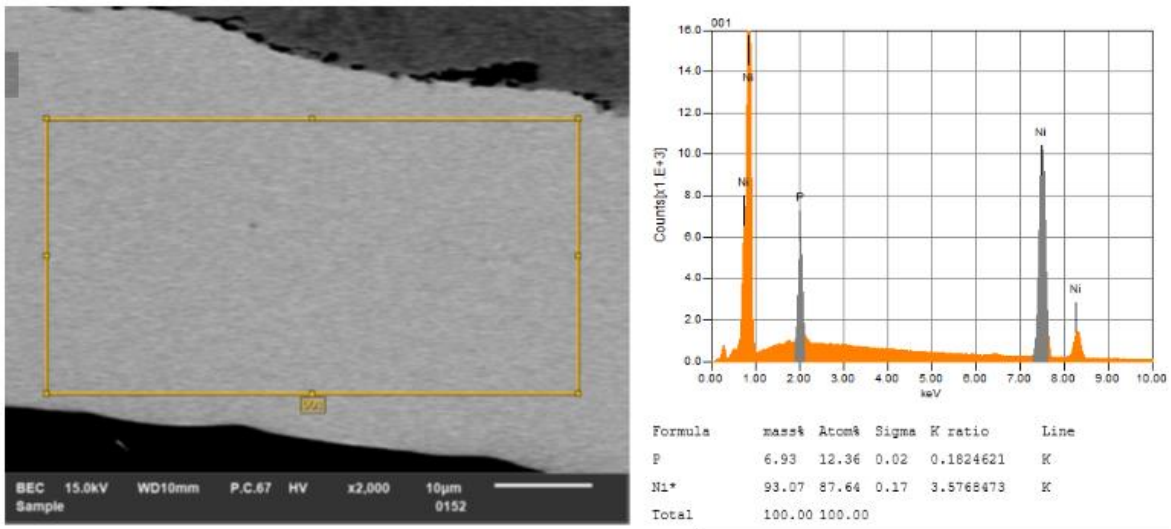

Figure 8. EDS measurement of SN 36 electroless nickel plating.

3.4 ETCHING AND BLACKENING

The etching and blackening process followed the parameters outlined in Table 1. The procedure was detailed and reviewed by Environmental Health and Safety (EHS) to ensure that proper chemical handling precautions were taken. The test set-up shown in Figure 9 was arranged under a flow hood; proper PPE and secondary containment was used while handling the concentrated nitric acid solution. A 9 Molar nitric acid bath was generated by slowly mixing 573.3 mL of HNO_3 with 250 mL of 18 mΩ deionized water then achieving the desired volume and concentration by adding DI water until the solution reached 1000 mL. A hot plate and stirring pill heated the solution to the desired 40°C set-point. A beaker of DI water was kept at room temperature, approximately 20°C.

Each sample was etched and blackened by suspending the EN plated samples in the nitric acid bath using steel wire. An example is shown in Figure 10. (The majority of the samples had a through hole in one corner that the wire was threaded through. Samples with SN ≤10 did not have this feature and were held by looping the wire around two opposing corners.) During the etching process, the samples change from their initial bright and shiny appearance to black in only a few seconds. The etching reaction creates a cloud of gaseous bubbles that move up to the surface of the bath and escape. After the required immersion time (nominally 40 s), the samples were immediately removed from the solution and rinsed in the DI water for approximately 30 s. The samples were allowed to air dry.

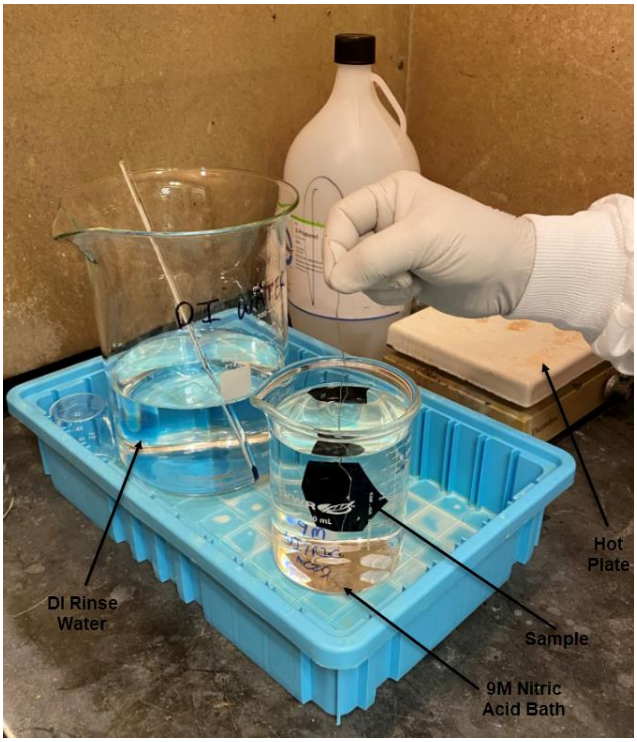

Figure 9. Nitric acid etch test set-up.

Figure 10. EN plated sample suspended with steel wire.

Next, the samples were visually inspected to record observations of the surface uniformity, defects, specularity, and qualitative assessment of the absorptivity ("blackness") of the surface. Each sample was

again weighed to estimate the remaining coating thickness. The XRF instrument measured the composition of the etched EN plating, with the caveats discussed above in Section 3.3. Finally, a sub-set of samples was evaluated using the SEM to view the surface morphology in order to provide additional insight into differences between samples. Figure 11 illustrates the conical pores that are created in the EN plating. The diameters of these pores are approximately 10 µm. This structure is very similar to the finding reported by Brown, Brewer & Milton.

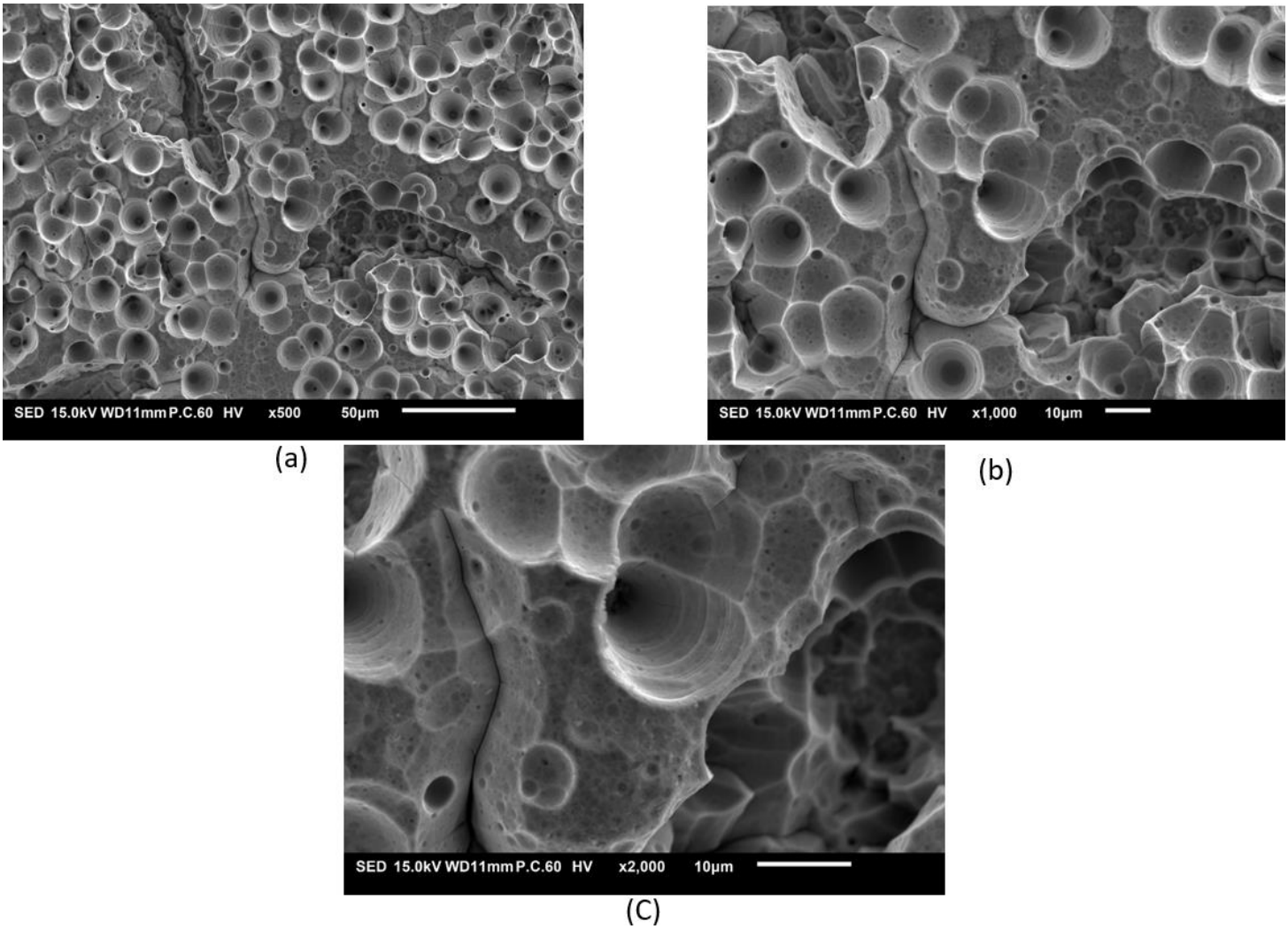

Figure 11. Post-etch surface morphology of sample SN 35. (a) 500x (b) 1,000x and (c) 2,000x magnification.

3.5 RESULTS AND DISCUSSION

Twenty-eight of the thirty samples listed in Table 2 were blackened using this etching technique (SN 34 and 36 were cross-sectioned to characterize the EN plating and were not etched). While the tests did immediately demonstrated the feasibility of creating absorptive black surfaces, it became readily apparent that the process was highly inconsistent despite efforts to tightly control as many variables as possible as depicted in Figure 11. In the top row, five samples were etched sequentially using the same nitric acid solution. Visually, the leftmost sample appears darkest and most absorptive, while the rightmost sample is lighter and more specular (particularly when viewed at higher angles of incidence). Additionally, the etching process did not appear uniform across the small 1.5" square surface as seen with SN 33. This sample was intentionally etched for an additional 20 s. The EN plating at the center of the sample is completely removed revealing the Invar 36 substrate, while the outer edges are very black. Therefore, this set of samples indicated that additional process variables not initially considered had a significant impact on the resulting surface morphology. These other parameters include sample orientation, sample agitation, initial sample temperature, and duration of time between the electroless nickel plating process and the etching process. The impacts of these variables are discussed below.

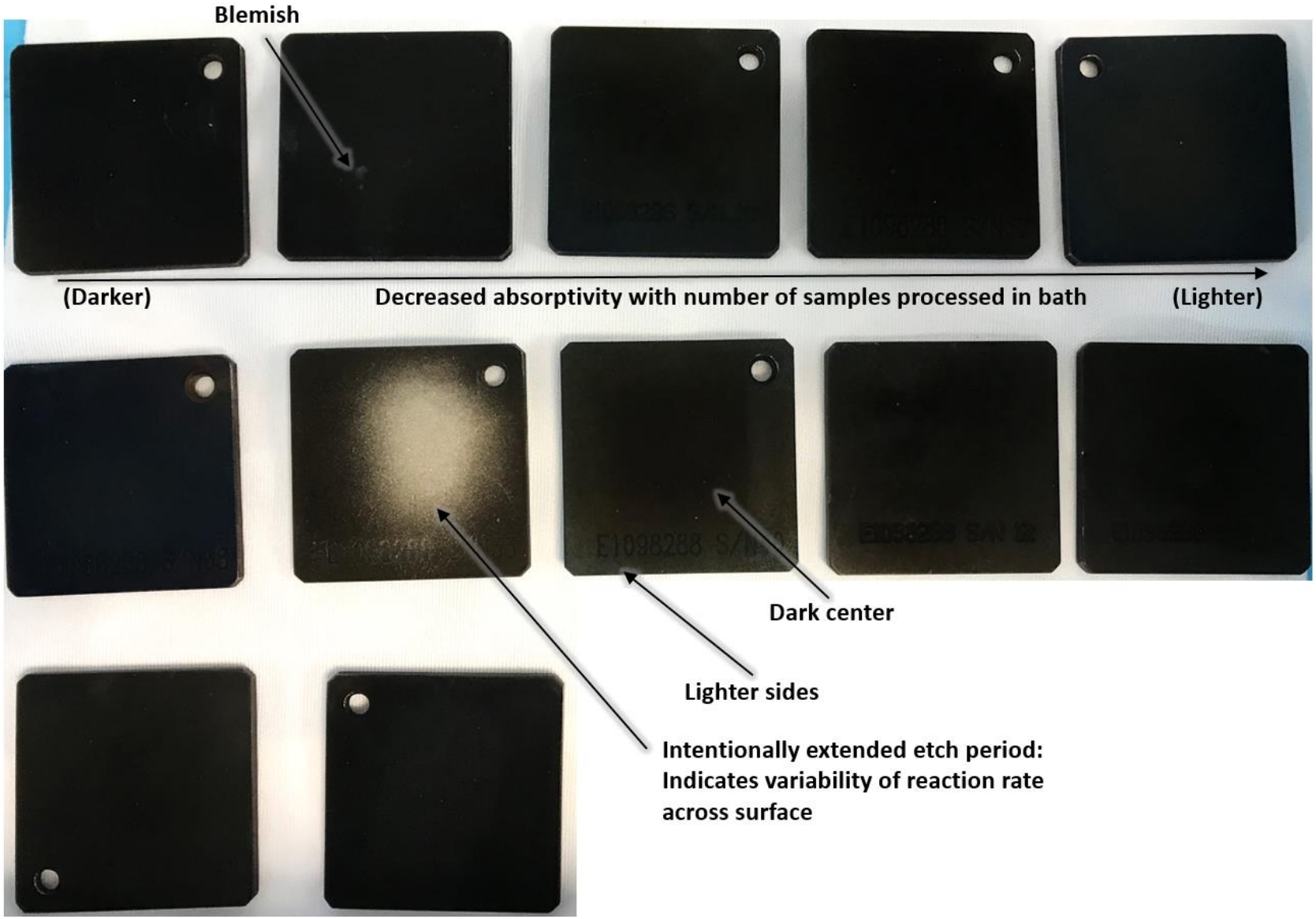

Figure 12. EBEN samples demonstrating process variability.

The pre- and post-etch mass of the samples, combined with the immersion time, allows the average etching rate for each sample to be estimated. For one set of four samples, Figure 13 quantifies a 33% decrease in the etching rate. As this etching rate decreases, less of the material is removed and the thickness of the remaining plating increases, which is indicated in the figure.

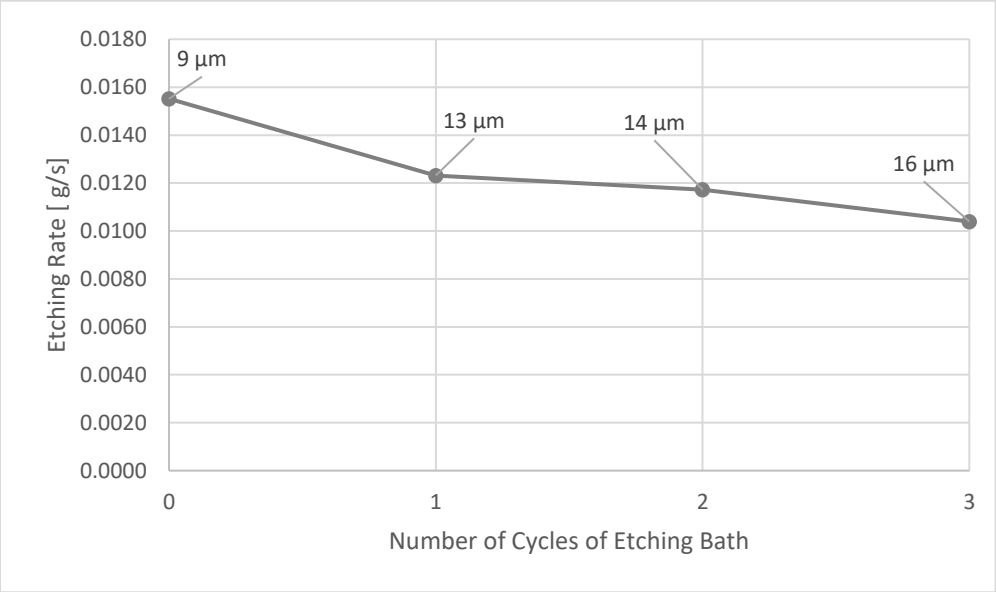

Figure 13. Change in etching rate with age of etching bath. Change in etching rate as the number of samples processed by the etching bath increases. The estimated final thickness of the etched plating is labeled for each sample.

The variability of the etch rate directly influences the resulting surface morphology. Figure 14 depicts the large number of intersecting conical pores that are created during the etching process when it occurs at a higher rate (0.0156 g/s) over the 40 s immersion time. These features trap the incoming light and prevent specular reflections to create a diffuse, matte surface. This can be contrasted with Figure 15, which had an etching rate of 0.0105 g/s with the same 40 s immersion time. The sample has significantly fewer conical features and large, smooth areas between groups of pores. These areas allow specular reflections from incoming light, which is undesirable for minimizing stray light in an optical system.

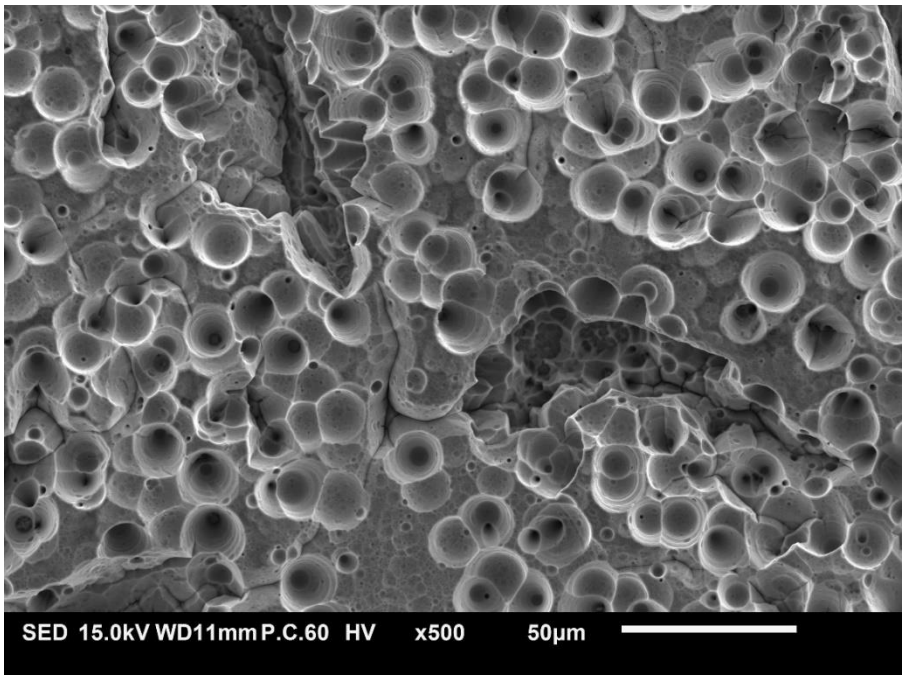

Figure 14. 500X SEM image of SN 35 with etch rate of 0.0156 g/s.

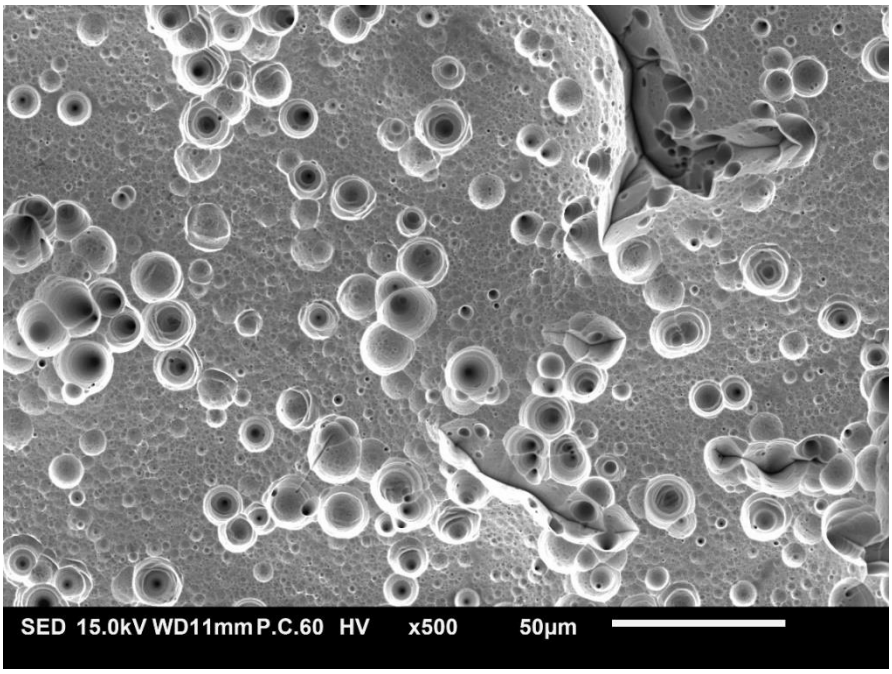

Figure 15. 500X SEM image of SN 23 with etch rate of 0.0105 g/s.

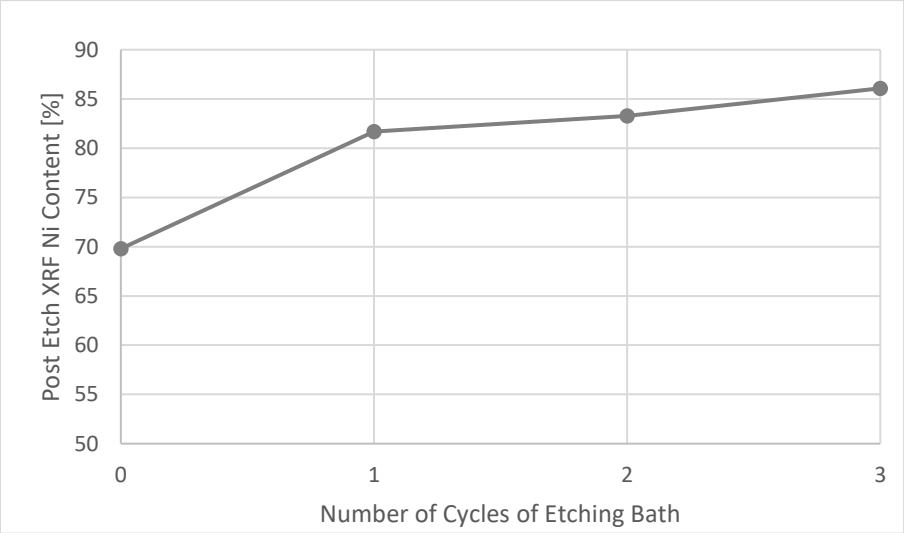

Figure 16. Change in post-etch nickel content with age of etching bath.

The change in etching rate correlated directly to the nickel content of the surfaces after blackening the samples (measured with the XL3T XRF). Figure 16 shows that as the age of the acid bath increases, the etching rate decreases, and the final nickel content increases. This is consistent with findings in the literature indicating that the etching process selectively attacks the nickel elements to create the conical pores in the surface. As discussed in Section 3.3, these measurement can only provide a qualitative comparison due to the ~10-20 µm coating thickness.

This variable could potentially be removed by only using a fresh etching solution for each part, or by using a significantly larger volume relative to the part size. Either option would generate a large amount of hazardous waste and be undesirable if blackening more than just a few parts. Alternatively, it might be possible to calibrate this effect and adjust the immersion time for each sample depending on the age of the bath. The geometry and surface area of the part will affect how quickly the solution ages, and this calibration would likely require intermittently measuring the bath composition. An investigation into this process was outside the scope of this work.

Since one of the goals of this investigation was to leverage the electroless plating capabilities of local vendors, the etching process did not occur immediately after plating. The duration between these two steps ranged from a couple weeks to a few months due to scheduling constraints. Similar to the effect of the nitric acid solution aging over time, the etching rate also appeared to decrease as this delay between process steps increased (Figure 17). It is hypothesized that this is the result of oxidization occurring on the surface of the

samples over time. After the EN plating process, all samples were sealed in bags with dry nitrogen intending to mitigate any oxidization, but it is possible that procedure was not sufficient. (A review of the literature did not indicate the time duration between plating and etching used by other groups to achieve their results. It is assumed to have occurred in close succession.) An additional processing step was evaluated by "pre-washing" samples in a much milder 1 M nitric acid solution at 40°C for 60 s to remove any potential oxidization build-up on the EN plating. After the pre-wash, the samples were immediately submerged in the 9 M solution to complete the blackening process. Qualitatively, this appeared to improve the uniformity and repeatability of the blackened surfaces, but the effect of this step was not fully quantified.

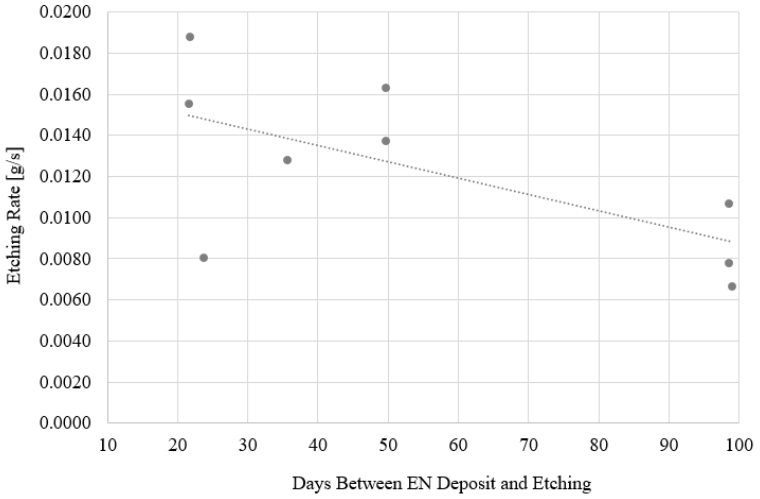

Figure 17. Decrease in etching rate with increase in days since en plating.

Upon completing the etching process and rinsing the parts in DI water, a thin black powder was typically deposited uniformly across the part. This initially gave the samples the appearance of having a uniform, absorptive, and diffuse surface. However, this deposit was easily wiped off with a cloth or removed by submerging the sample in an ultrasonic DI bath. Figure 18 shows the black deposit intact on the right side of the sample, while the left side of the image shows the surface once the deposit is wiped off. This result is consistent with observations from Saxena, Rani, & Sharma who report that a powdery, nickel-phosphorous black oxide develops during the oxidation reaction but does not adhere. Because of the uniformity and absorptivity of this deposit, some consideration was given to the possibility of binding the black-oxide powder to the surface. However, it is likely that any additional "clear-coat" added to the surface would compromise the promising optical properties and present additional challenges for space qualification.

Figure 18. Black oxide deposit on surface of sample. Left side of image - deposit removed by wiping area with a clean, lint free cloth.

4. PROCESS APPLICABILITY

Additional testing was conducted to determine the effects of larger surface area, different substrates, and geometry that is more representative of flight parts at MIT LL. These tests were not controlled as rigorously as the experiments conducted in Section 3, but did provide insight into other challenges associated with practical implementations of this blackening technique.

4.1 LARGE FLAT PANELS

A set of 3" x 5" x 1/32" Invar 36 flat panels were fabricated to understand how this process scales to larger surface areas. The panels were media blasted with 60 grit AlO_2, plated with electroless nickel, and blackened using the same nominal parameters outlined in Table 1 except with the addition of the 1 M, 40°C nitric acid "pre-wash" for 30 s (see Section 3.5). These tests revealed significant color gradation across the surface of the samples with some regions appearing darker and others lighter. Similar to the "over-etched" sample in Figure 12, this indicates that the etching process does not necessarily occur uniformly across the surface. In addition, numerous speckles are scattered across the surface, which may be a result of bubbles or turbulence in the acid bath as the rapid reaction occurs. This variability could potentially be mitigated by increasing the size of the acid bath, continually mixing/stirring the solution, or agitating the sample to ensure the oxidization reaction occurs evenly over all surfaces.

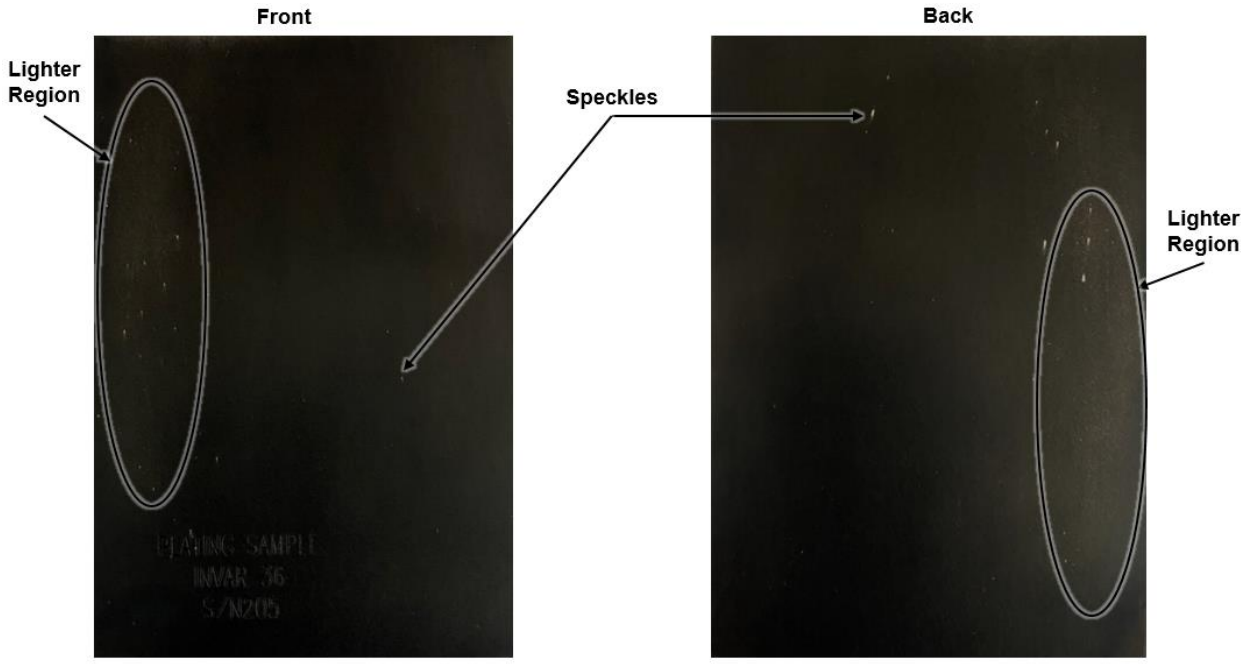

Figure 19. EBEN Invar 36 flat panel.

4.2 TESTING WITH DIFFERENT SUBSTRATES

Since MIT LL prototypes typically use a variety of materials, it is important to understand how different substrates affect this process. Similar to the samples in Section 4.1, a set of 3" x 5" x 1/32" panels were fabricated from Aluminum 6061-T6. The surface prep, electroless plating, and blackening process were the same as the samples in the previous Section 4.1. Figure 20 shows striking variability across the part despite using the same nominal process parameters as the sample shown in Figure 19. The bottom edge of the panel was toward the bottom of the nitric acid bath and the top edge toward the surface. The off-gassing from the oxidization reaction appears to effect the reaction rate and it travels across the surface of the part to the top of the bath. The etching reaction occurs more rapidly toward the top of the part as the electroless nickel is fully removed revealing the aluminum substrate below. This work did not investigate the variability between the Invar 36 and Aluminum 6061-T6 results any further, but noted that process development will be required for each substrate material.

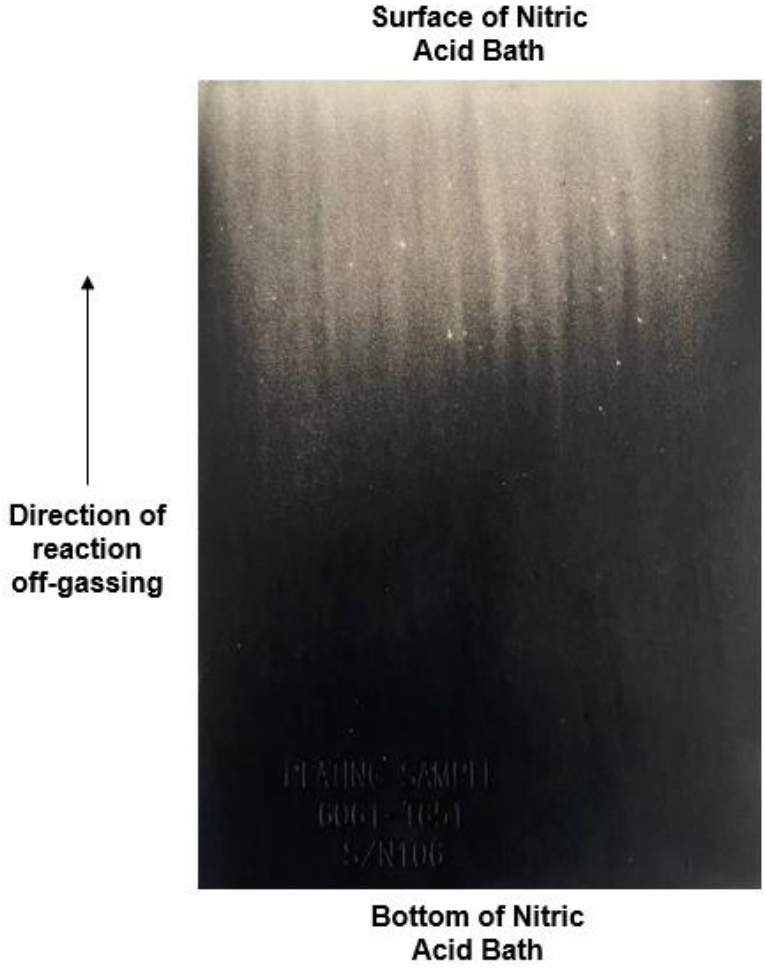

Figure 20. EBEN aluminum 6061-T6 flat panel.

4.3 REALISTIC GEOMETRY

It was also necessary to understand the implications of moving from flat surfaces to geometry more representative of parts used in flight optical systems. A clam-shell "stray-light bore" was designed, which was made up of two Invar 36 parts (Figure 21). The surface preparation, electroless plating, and blackening were all conducted with the two parts assembled together, as shown in Figure 22 and Figure 23, using the same nominal process parameters from Table 1 and without the additional pre-etch step.

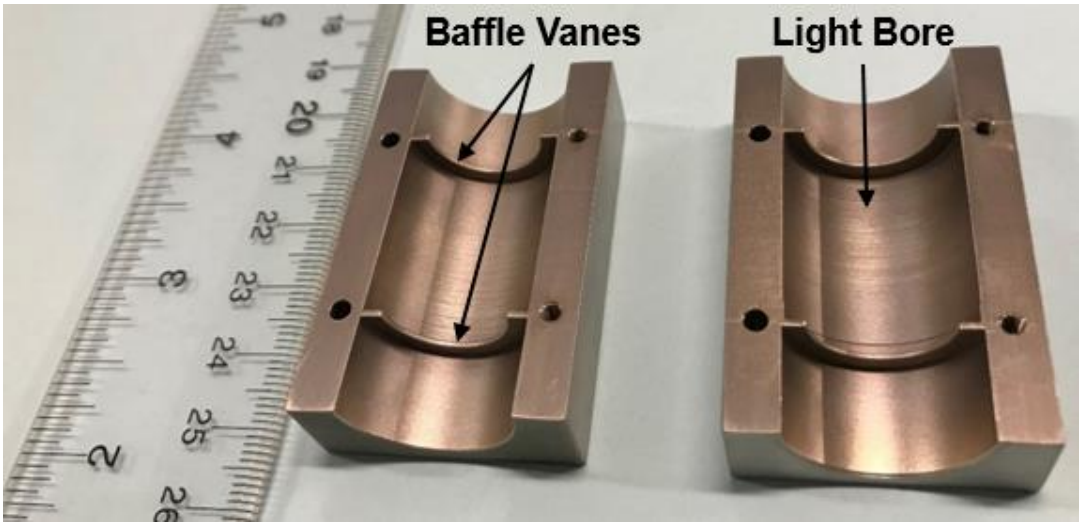

Figure 21. Invar 36 clam-shell stray light bore. Part number: E111354.

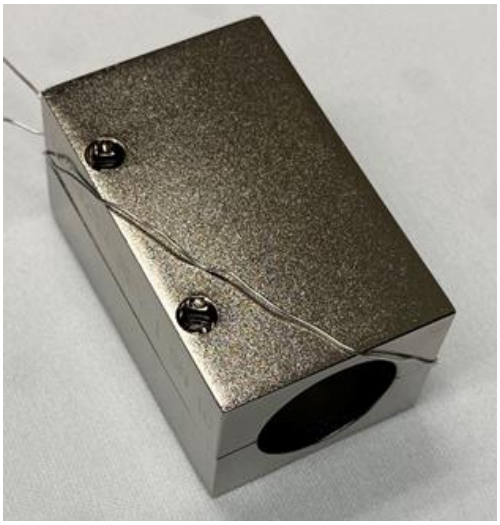

Figure 22. Assembled stray light bore plated with electroless nickel.

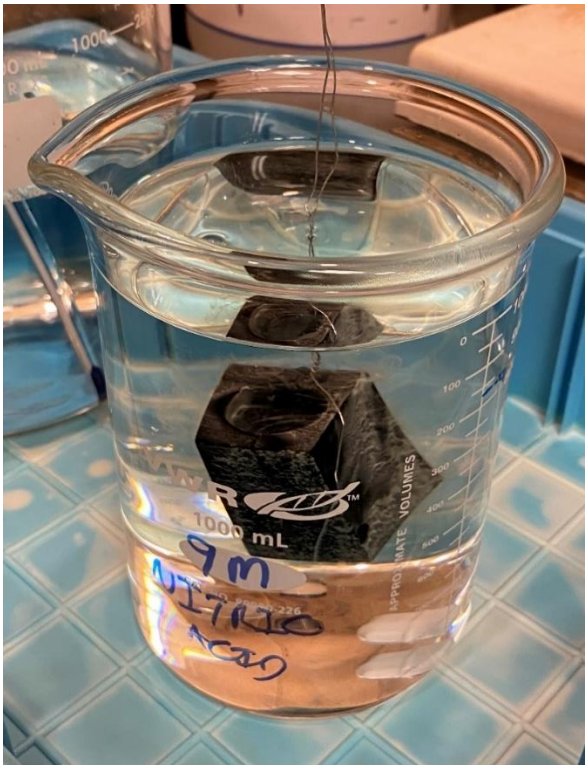

Figure 23. Assembled stray light bore submerged in nitric acid solution.

The parts were disassembled to inspect the interior surfaces to determine the uniformity of the reaction inside internal cavities and in the presence of features such as baffle vanes. Figure 24 and Figure 25 indicate that the etching reaction does occur inside the bore, but is not uniform across all surfaces. Lighter and more specular regions are present next to darker and more absorptive areas. Corners at the base of baffle vanes also appear very shiny. These irregularities are undesirable for optical systems that require high performance stray light suppression. These features make generating accurate predictions from analytical stray light models difficult. Each part will also behave differently and could create unexpected glints or background structure on a system's detector.

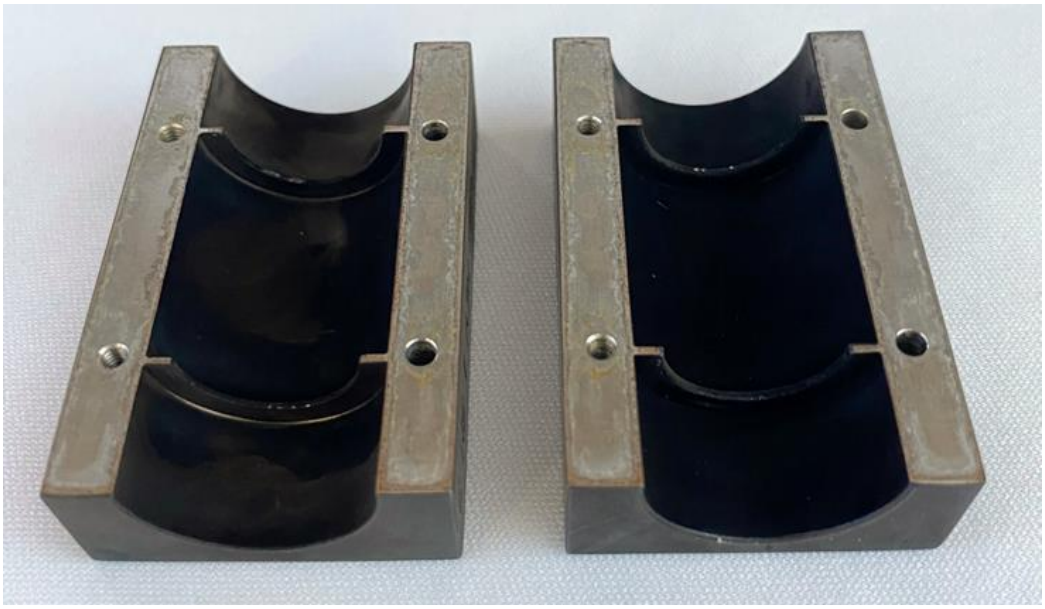

Figure 24. Disassembled stray light bore after blackening. (Left) Part cleaned with DI water ultrasonic bath. (Right) Part only rinsed in DI water leaving black oxide deposit intact.

Figure 25. One half of stray light bore. Image shows lighter specular regions, darker absorptive regions, and specular corners at the base of the baffle vanes.

4.4 ALTERNATIVE BLACK ELECTROLESS NICKEL APPROACH

An additional blackening approach was explored because of the process variability presented in Sections 3 and 4. As mentioned in the literature review, Jin, Yang, Zeng, & Fu, (2015), conclude that an anodic oxidation process with H_3PO_4 (phosphoric acid) is a superior blackening process compared to the nitric acid etching reaction, which has been discussed up to this point. Their results indicate that this process creates a finer array of uniform, conical cavities approximately 1-3 µm in diameter. They optimized a set of process parameters to minimize the surface reflectance and any surface defects, and the values are presented in Table 3. In the visible range (400 – 760 nm), they achieve reflectance values as low as 0.14% (2015, p. 8).

Table 3

Anodic Oxidation Test Parameters

Parameter	Value	Units
Plating Thickness	50	µm
Phosphorous Concentration	6-9	% by Mass
Anodic Bath Composition	Phosphoric Acid [H_3PO_4]	-
Anodic Bath Voltage	40	V
Immersion Time	40	Min

Given the explicit claims that this alternative blackening method mitigates the challenges detailed throughout this report while achieving increased stray light performance, it was prudent to investigate further. Since this is an anodic process, it requires additional equipment that was not on hand at MIT LL. Therefore, the plating vendor AOTCO was utilized. Eight samples with the parameters listed in Table 4 were fabricated. The sample surfaces were prepared at MIT LL then delivered to AOTCO to complete the electroless nickel plating and this alternative blackening step. The parts were rinsed in DI water for 40 s to complete the process. The samples were returned to MIT LL for evaluation.

Table 4

Sample Parameters Used with Anodic Oxidation Process

Sample SN	Size	Material	Surface Preparation
101	3” x 5” x 1/32”	Aluminum 6061-T6	50 Grit Steel Shot
102			60 Grit AlO_2
103			#8 Glass Beads
104			#13 Glass Beads
201		Invar 36	50 Grit Steel Shot
202			60 Grit AlO_2
203			#8 Glass Beads
204			#13 Glass Beads

Figure 26. Samples blackened with alternative anodic oxidation. (Left) SN 101 aluminum panel (Right) SN 201 Invar 36 panel.

The two samples shown in Figure 26 demonstrate that this alternative process does create black, absorptive surfaces. Unfortunately, significant color gradiation is still present and across all of the panels. In addition, all of the Invar 36 samples appear to have significant crazing in the coating, which can be seen in the image of SN 201. The coarse 50 grit media blast provided the most diffuse result with the other surface treatments leading to much more specular surfaces. This blackening method does show some potential, but the results did not meet the expectations set by the published research.

4.5 SINGULARITY BLACK LT AERO

During the research review for this effort, a different black coating was discovered, which has significant potential for near-term implementation at MIT LL. While this work specifically evaluated black electroless nickel coatings, the ultimate goal was to find alternative black coating options with fewer compromises compared to those typically used in MIT LL payloads. To that end, information regarding Singularity Black LT Aero is provided here to motivate future evaluation.

This coating is a carbon nano-tube impregnated black paint that forms a porous, 3D network on the surface of the part. The vendor for this product is NanoLab Inc, located in Waltham, MA. It was originally developed under a NASA Small Business Innovation Research (SBIR) grant in 2011 and is now in its second generation of formulation. Optically, the coating performance exceeds almost all commercial products and has total hemispherical reflectance that is <1.5% over the VIS-NIR range. The coating is low outgassing and has been vibration tested and thermal cycled to demonstrate its suitability for the space environment. The paint is substrate agnostic and does not require specific surface preparation or primers. Finally, NanoLab's in-house painting service provides short lead times, is low cost, and is capable of working with complex geometries. Additional detail is found in NanoLab's technical datasheet.

Because of the promising properties of this coating for space flight applications, two additional parts with the "realistic geometry" shown in Section 4.3 were assembled and delivered to NanoLab. The painting process was completed in less than four days for a cost of under $200. The parts, shown in Figure 27, were disassembled and inspected at MIT LL. The interior surfaces were uniformly painted and the surfaces were extremely diffuse and absorptive. To independently verify the optical performance, NanoLab provided a 2" square sample on a 304 stainless steel substrate for optical characterization. The results are provided in Section 5 and compared to the results achieved using the processes described above.

Figure 27. Stray light bore painted by NanoLab with Singularity Black LT Aero.

5. OPTICAL CHARACTERIZATION

5.1 MATERIALS AND METHODS

The Optical Materials Measurement Range (OMMR) operated by Group 38 at MIT LL characterized the stray light control coatings discussed in this work. These measurements serve to provide a comparison of optical performance to inform decisions for particular applications or avenues for further investigation. The measured samples are listed and described in Table 5. Sample 215 is an additional black electroless nickel plating that provides a reference for the optical performance that a commercially available black EN surface can provide. The sample was produced by AOTCO using the following drawing notes, which were developed in collaboration with MIT LL for use on a Lincoln program.

- FLASH ENTIRE PART WITH ELECTROLESS NICKEL TO 0.001" MAX THICKNESS.
- UNIFORM, MATTE, BLACK NICKEL PLATE TO MAX THICKNESS OF 0.0007".

  APPLY AIR ABRASION WITH ALUMINUM OXIDE BEFORE NICKEL OXIDATION

  TO REACH DESIRED MATTE FINISH. ENSURE NO COLORATION.

Sample 31 is an etched black electroless sample that was both plated and blackened in 2018 by AOTCO (using the same parameters from Table 1) during the original process investigation under the Mustang program. This sample was very uniform, absorptive, and diffuse; it represents the “highest quality” surface generated using nitric acid oxidation.

Table 5

Samples Optically Characterized at the MIT LL OMMR

Sample SN	Description	Size	Substrate
215	AOTCO Black EN	3” x 5”	Invar 36
31	AOTCO EBEN (2018)	1.5” x 1.5”	Invar 36
28	MIT LL EBEN (Small Coupon)	1.5” x 1.5”	Invar 36
205	MIT LL EBEN (Flat Panel)	3” x 5”	Invar 36
10	MIT LL EBEN w/ Oxide Layer	1.5” x 1.5”	Invar 36
101	AOTCO Black EN using Anodic Etch	3” x 5”	Aluminum 6061-T6
SB	NanoLab Singularity Black Lt Aero	2” x 2”	304 SS

The OMMR conducted direction hemispherical reflectance (DHR) measurements over a broadband range (500-1900 nm) at near normal incidence. The bidirectional reflectance distribution function (BRDF) was also measured using a 1064 nm source at 5, 30, and 60 deg angles-of-incidence (in-plane only). This measurement captures the scattering characteristics of a particular surface to determine how specular or diffuse a surface is at different AOI.

5.2 RESULTS AND DISCUSSION

The Directional Hemispherical Reflectance measurements for three etched black electroless nickel sample are presented in Figure 28. The reflectance of SN 31 is below <1% in the wavelength range of 500 to 950 nm. Out to 1650 nm, the reflectance of the sample remains below <1.5%. These results demonstrate the exceptional performance that can be achieved using this technique. However, the measurements for SN 28 and SN 205 quantify the variability of the process. For example at 1000 nm, SN 31 has a reflectance of 1%, SN 28 is 2.5%, and SN 205 is 5%. These inconsistent results create significant challenges for predicting the “as-built” performance of an optical assemblies’ stray light control system, which in turn, can impact whether or not other system requirements are met.

The DHR measurements for all the samples listed in Table 5 are presented in Figure 29. The EBEN sample SN 31 compared very closely to the NanoLab Singularity Black paint, which is one of the most

absorptive commercially available coatings. The reflectance values of SN 10 indicate that the thin, black oxide layer deposited during the etching process is also very absorptive. Unfortunately it is fragile and easily wiped off, which can reveal under-etched surfaces, such as SN 28 and 205, with significantly higher reflectance. The sample blackened with the anodic oxidation process, SN 101, presented the highest reflectance values. Finally, SN 215 with a commercially available black EN was <3.5% reflective out to 1750 nm.

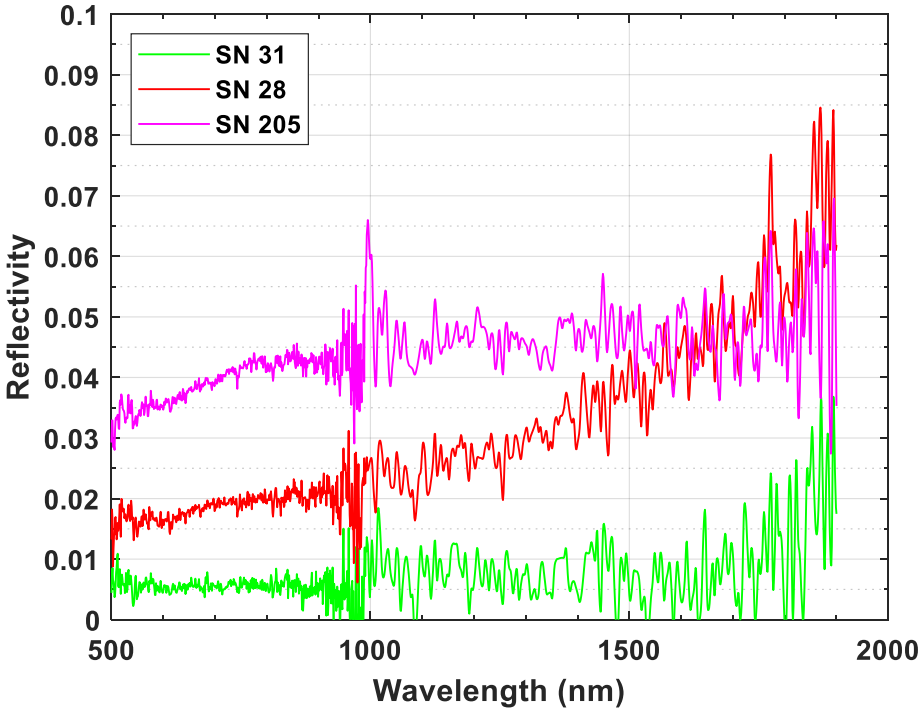

Figure 28. Directional hemispherical reflectance of EBEN coatings.

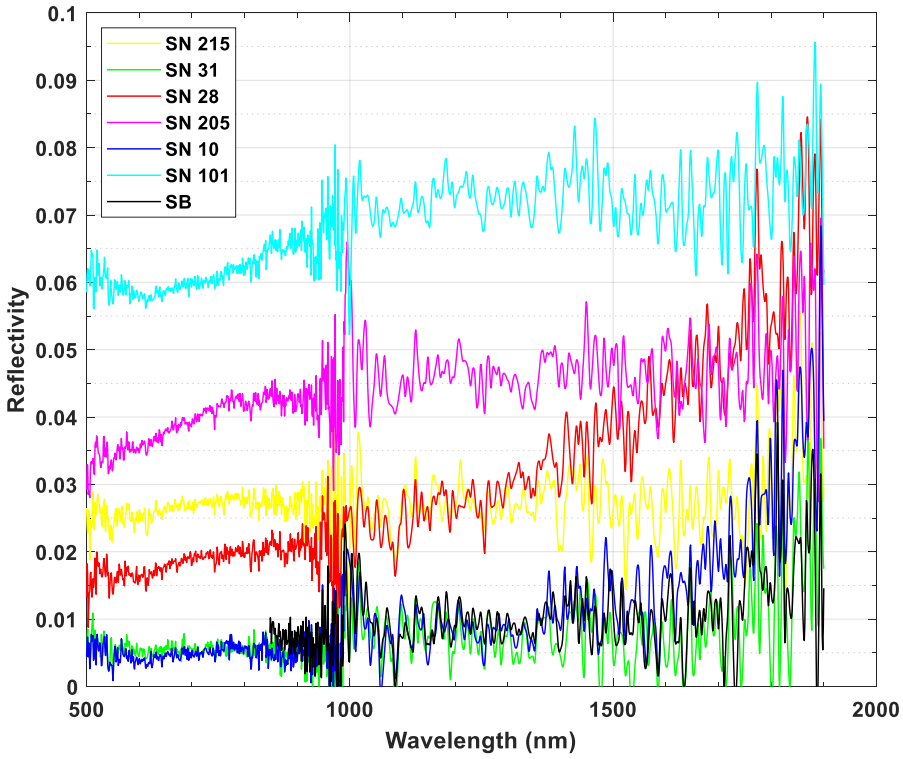

Figure 29. Summary of directional hemispherical reflectance of all samples.

The bidirectional reflectance measurements for all samples are provided in Figure 30 for P-polarization and S-polarization. The majority of the samples have significant specular components at all three angles of incidence, as noted by the peaks at 5, 30, and 60 degrees. Notably, SN 31 (green data points) again compares similarly to the Singularity Black paint (black data points), and both are significantly more diffuse at each AOI than the other samples. These highly diffuse coatings are often necessary for stray light control since they limit the amount of undesired light that reflects and propagates forward off the surface, which can create image obscuring glints, for example. By comparing the scale of the two sets of figures, it is also apparent that there are polarization effects present. Depending on the parameters of a specific system, these effects may need to be considered and further characterized before implementation.

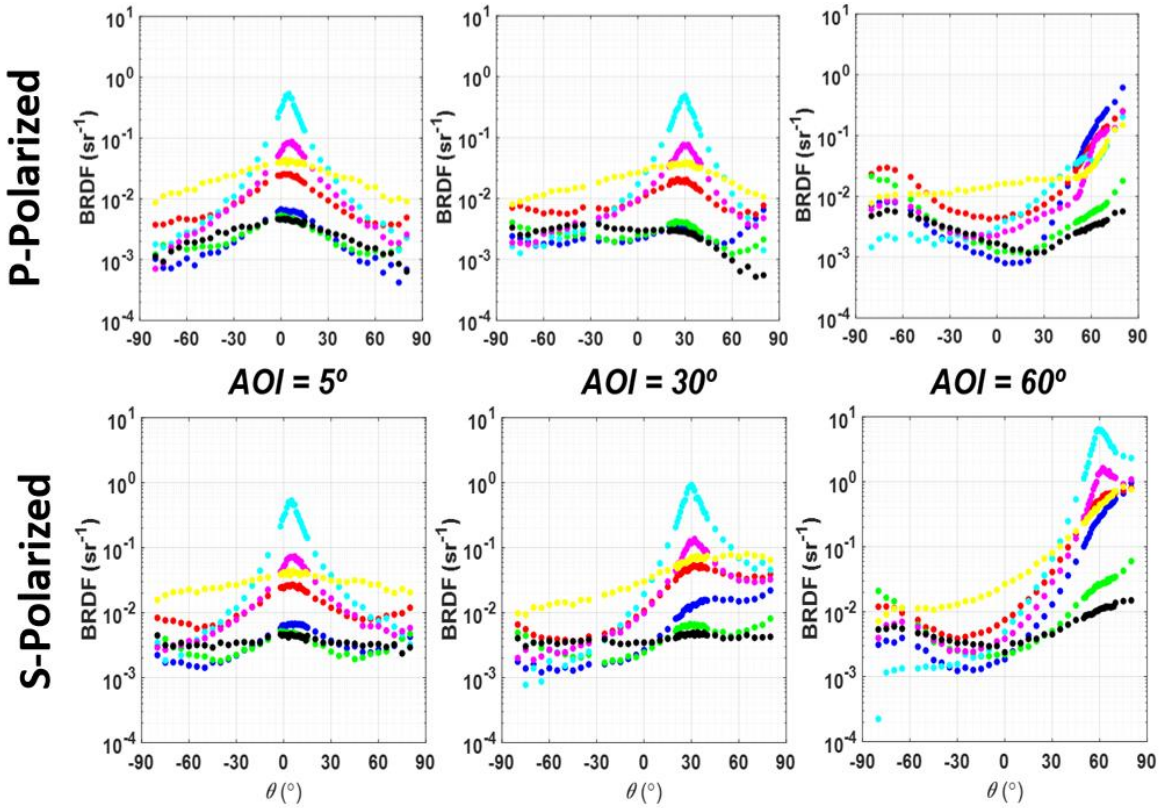

Figure 30. Bidirectional reflectance measurements of samples. See legend in Figure 30. Forward (θ > 0º) and backward (θ < 0º) scatter.

This page intentionally left blank.

6. CONCLUSION

This work explored the viability of developing a robust process for creating ultra-black electroless nickel coatings. A nitric acid oxidation process selectively attacks the elemental nickel in the Ni-P coatings to create a surface micro-structure that can be very absorptive and diffuse. The promising results from this process have been published by outside research groups and have also been demonstrated at MIT LL. The optical characterization results confirm that this technique can create surfaces that are three to four times more absorptive than commercially available black EN coatings. This performance improvement could significantly benefit systems at MIT LL that need stringent stray control to meet SNR requirements at sensitive detectors.

Unfortunately, as outlined in this report, the repeatability, scalability, and applicability of this blackening technique is extremely challenging. Despite rigorously controlling and monitoring numerous parameters, variability in the EN plating process and non-uniformity of the oxidation reaction contributed to the inconsistent results presented. Additional research could be conducted to further minimize these variables, such as standing-up an in-house EN plating capability to control and optimize that portion of the process. However, this would require a significant investment and may only resolve some of the difficulties observed. An additional blackening technique using anodic oxidation was also evaluated, but it did not produce surfaces that exceeded already commercially available options.

Despite these unsatisfactory results, an additional stray light coating option was uncovered during the course of this work. Singularity Black LT Aero, provided by NanoLabs in Waltham, MA, is extremely absorptive and very diffuse as demonstrated in the DHR and BRDF results. This carbon nanotube impregnated black paint is designed for use in airborne and space environments. It is also very inexpensive and can be procured with short lead times. Because of these characteristics, it has the potential to significantly benefit future MIT LL programs that require high performance stray light coatings, and is worth further investigation and characterization.

This page intentionally left blank.

7. ACKNOWLEDGEMENTS

The authors would like to thank Dr. Todd Mower, Dr. Vishwa Shukla, and Andrew Kopanski for contributing SEM images and EDX measurements of the sample surface preparation, electroless nickel cross-section & surface, and the blackened surface microstructures. Dr. Michael Pasqual and the Group 38 OMMR were instrumental in conducting the optical characterization of the samples. Finally, thanks to Jim Lincoln for managing the required sample and supply procurements.

This page intentionally left blank.

REFERENCES

1. Brown, R. J., Brewer, P. J., & Milton, M. J. (2002). The physical and chemical properties of electroless nickel-phosphorus alloys and low reflectance nickel–phosphorus black. Journal of Materials Chemistry, 2749-2754. Retrieved 10 16, 2017.

2. Geikas, G. I. (1983). Scattering Characteristics Of Etched Electroless Nickel. Proc. SPIE 0384, Generation, Measurement and Control of Stray Radiation III. Los Angeles: SPIE. doi:10.1117/12.934932.

3. Jin, Y., Yang, K., Zeng, X., & Fu, Q. (2015). A Novel Blackening Method of Preparing Ultra-Black Ni-P Coatings: Effect of Process Parameters on Morphology. Surface Review and Letters, 22, 1550017 (8 pages). doi:10.1142/S0218625X15500171.

4. Johnson, C. (1980). Black electroless nickel surface morphologies with extremely high ligh absorption capacity. Metal Finishing, 78(7), 21-24. Retrieved 2 14, 2018.

5. Saxena, V., Rani, R., & Sharma, A. (2006). Studies on ultra low reflectance black electroless nickel on invar. Galvanotechnik, 97, 827-840. Retrieved 2 27, 2020.

This page intentionally left blank.